Protease-resistant TDP-43 in ALS and FTLD with frontotemporal dementia-43 pathology

These different banding patterns in TDP-43 proteinopathies may represent different conformations of abnormal TDP-43 or their aggregates. To test this hypothesis, we subjected the abnormal TDP-43 recovered in the sarkosyl-insoluble pellets to protease treatment and analysed the protease-resistant bands. Proteins can be easily cleaved by proteases if they are denatured or unstructured, but domains that have rigid structures, such as a β-sheet conformation or that are structurally buried or interacting with other molecules, are highly resistant to proteases. On trypsin or chymotrypsin treatment, the full-length 45-kDa band and the smearing substance of TDP-43 disappeared, leaving protease-resistant fragments at 16–25 kDa (Figs 4 and 5). As expected, the protease-resistant banding patterns were different and distinguishable into three patterns (Figs 4 and 5). In ALS, trypsin-resistant doublet bands at 16 and 15 kDa, and two minor bands at ~24 kDa were detected, whereas a single band at 16 kDa and some additional bands at ~24 kDa were detected in FTLD-TDP type A (Fig. 4A, Lanes 1 and 2). In FTLD-TDP type B, the same banding pattern as that in ALS was observed (Fig. 4A, Lane 3). In FTLD-TDP type C, a broad single band at 16 kDa and some additional bands at ~24 kDa were detected (Fig. 4A, Lane 4). No such bands were detected in Alzheimer's disease (Fig. 4A, Lane 5).

Similarly, on chymotrypsin treatment, multiple protease-resistant bands were detected at 16–25 kDa and the chymotrypsin-resistant band patterns were also different between the three disease subtypes (Fig. 4B). Doublet bands were seen in ALS and FTLD-TDP type B, but only a single band in FTLD-TDP type C was detected at ~16 kDa (Fig. 4B). In FTLD-TDP type A, the lower band (15 kDa) of the ~16 kDa doublet was more intense than the upper one (16 kDa).

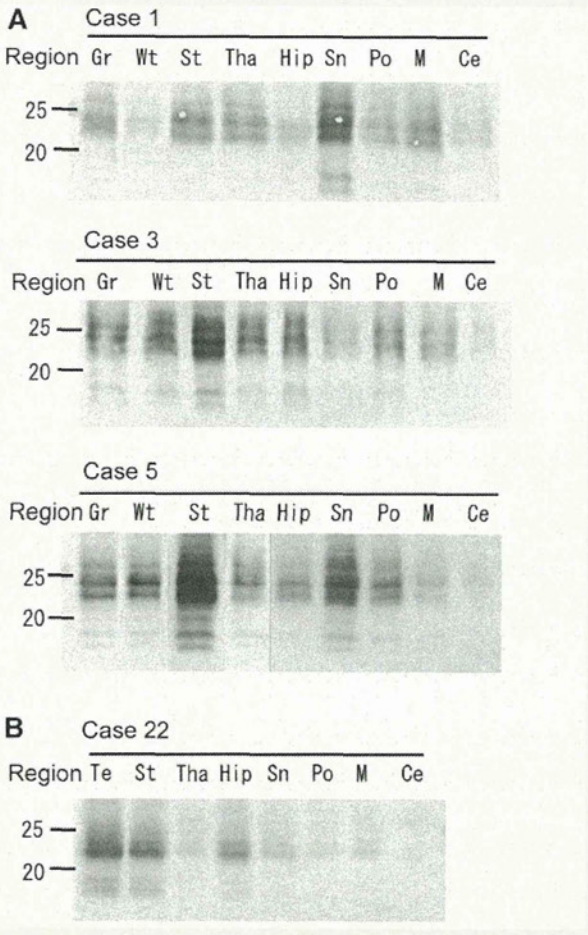

Figure 3 Immunoblot analyses of the C-terminal fragments of phosphorylated TDP-43 in the different brain regions of cases with ALS (Cases 1, 3 and 5, as shown in Fig. 1) (**A**) and FTLD-type C (Case 22, as shown in Fig. 1) (**B**). (**A**) Immunoblots of insoluble TDP-43 in the grey or white matter of precentral cortex, striatum, thalamus, hippocampus, substantia nigra, pons and medulla of ALS cases. (**B**) Immunoblot of TDP-43 in temporal cortex, striatum, hippocampus, thalamus, substantia nigra, pons and cerebellar cortex of the case with FTLD-TDP type C. Ce = Cerebellar cortex; Gr = grey matter of precentral gyrus; Hip = hippocampus; M = medulla; Po = pons; Sn = substantia nigra; St = striatum; Tha = thalamus; Te = temporal cortex; Wt = white matter of precentral gyrus. Immunoblots of spinal cords of cases with ALS are shown in Fig. 1.

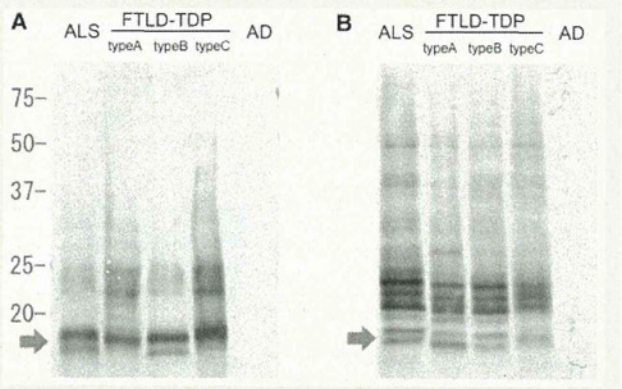

Figure 4 Immunoblot analysis of phosphorylated TDP-43 from representative ALS and FTLD-TDP cases after protease treatment. (**A**) Immunoblot of insoluble TDP-43 from cases with ALS, FTLD-TDP type A, type B, type C and Alzheimer's disease (AD) after trypsin treatment. Doublet bands at ~16 kDa (arrow) and some minor 23–24 kDa bands are detected in ALS and FTLD-TDP type B, whereas a single band at ~16 kDa and several bands at 23 and 24 kDa are detected in FTLD-TDP type A and type C. No such bands are detected in the Alzheimer's disease case. (**B**) Immunoblot of insoluble TDP-43 from cases with ALS, FTLD-TDP type A, type B, type C and Alzheimer's disease after chymotrypsin treatment. Multiple protease-resistant TDP-43 bands are detected at 16–25 kDa. Doublet bands at ~16 kD (arrow) are detected in ALS and FTLD-TDP type A and B, whereas a single band at ~16 kD (arrow) is detected in the case with FTLD-TDP type C. In FTLD-TDP type A, the lower band of the doublet at 16 kDa is more intense. No such bands are detected in the Alzheimer's disease case.

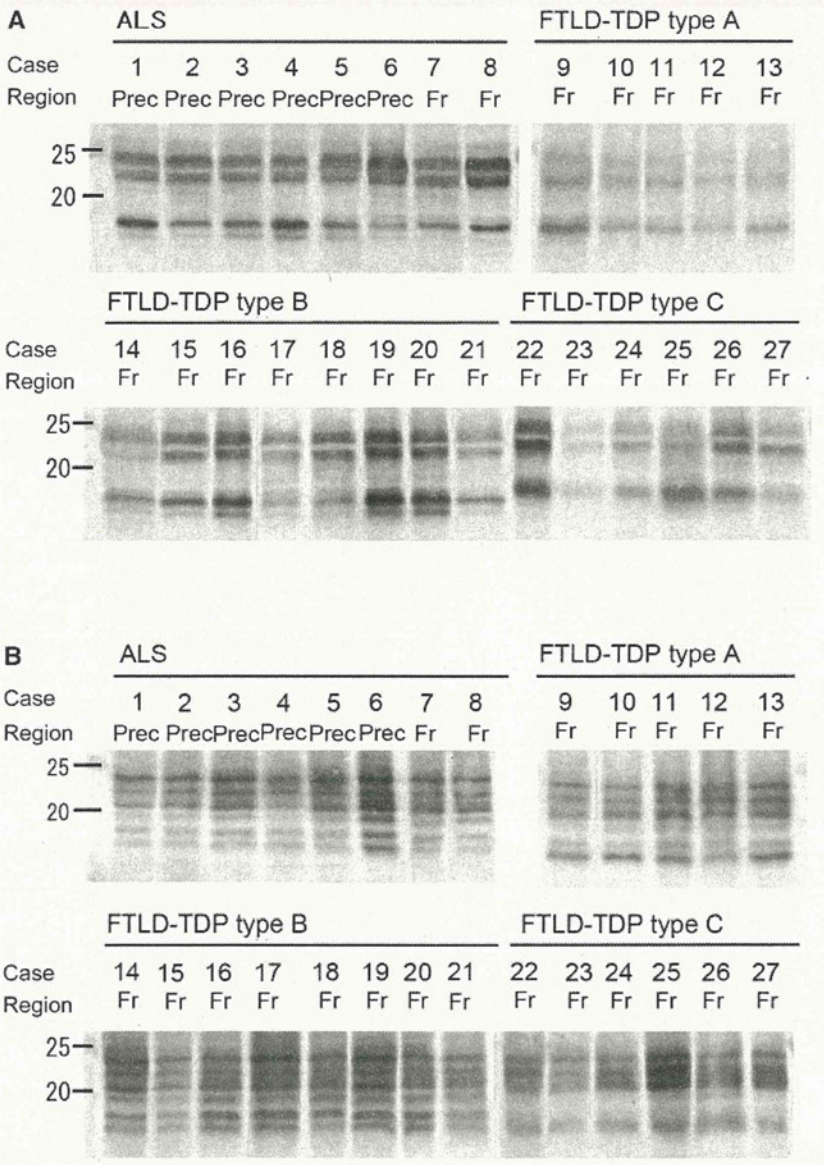

Figure 5 Comparison of the protease-resistant TDP-43 banding patterns in ALS and FTLD-TDP. Immunoblot analyses of trypsin-resistant (**A**) and chymotrypsin-resistant (**B**) fragments of TDP-43 from all cases examined. The banding patterns of ALS and FTLD-TDP type B cases are indistinguishable. Fr = frontal cortex; Prec = precentral gyrus.

In all cases examined, the trypsin-resistant banding patterns were clearly distinguishable between the disease subtypes in accordance with the three different types of banding pattern of TDP-43 C-terminal fragments, although it is difficult to distinguish the trypsin band pattern of type A from that of type C (Figs 5A, 6A and Supplementary Fig. 5). The chymotrypsin-resistant banding patterns were distinguishable and could be differentiated into three types (Figs 5B, 6B and Supplementary Fig. 6), also in accordance with the banding pattern of the TDP-43 C-terminal fragment. The banding patterns of ALS and FTLD-TDP type B were the same, whereas the banding pattern of FTLD-TDP type A was distinguishable from those of type C and type B (Figs 4 and 5). The combination analyses of trypsin and chymotrypsin-resistant banding patterns confirmed that TDP-43 proteinopathies can also be biochemically distinguishable into three types according to TDP-43 subtypes. These results strongly suggest that the different C-terminal banding patterns represent different conformations of TDP-43 aggregates and that the distinct types of TDP-43 are deposited in association with distinct pathological phenotypes of TDP-43 proteinopathies.

Immunoblot analysis using phosphorylation independent TDP-43 polyclonal and monoclonal antibodies detected some TDP-43 fragments in the ALS and FTLD-TDP cases after trypsin or chymotrypsin treatment, although no clear difference was observed in the banding patterns between ALS and other subtypes of FTLD-TDP (Supplementary Fig. 7). The distinctive

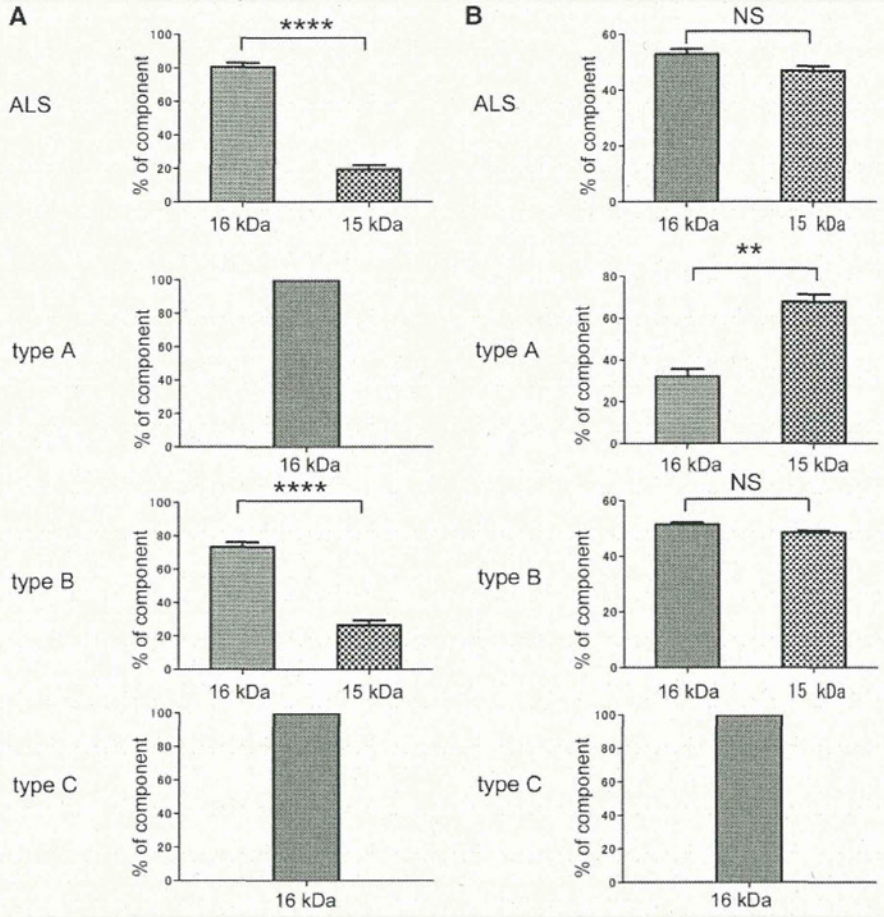

Figure 6 Quantitative analysis of protease-resistant ~16 kDa band. (**A**) The intensity of trypsin-resistant ~16 kDa band of each case was quantitated with ImageJ and statistically analysed. (**B**) The intensity of chymotrypsin-resistant ~16 kDa band of each case was quantitated with ImageJ and statistically analysed. Data indicate mean (SEM). ****$P < 0.0001$, **$P < 0.01$, NS = not significant.

protease-resistant bands at ~16 kDa of ALS were not detected with both phosphorylation independent antibodies (Supplementary Fig. 8).

We also analysed the banding pattern of phosphorylated TDP-43 in another series of five sporadic cases with TDP-43 pathology (Alzheimer's disease, Alzheimer's disease/dementia with Lewy bodies and Alzheimer's disease/argyrophilic grain disease) (Supplementary Table 1). The banding pattern of the C-terminal fragments, and trypsin- or chymotrypsin-resistant fragments, in these were same as those of FTLD-TDP type A with *GRN* mutation (Supplementary Fig. 9).

Mass spectrometric analysis of protease-resistant bands of TDP-43 in ALS and FTLD-TDP type C

To further investigate the differences in the abnormal TDP-43 protein species at a molecular level, we analysed the ~16 kDa trypsin-resistant bands by mass spectrometry. Mass analysis of chymotrypsin digests of ~16 kDa trypsin-resistant fragments identified 4 peptides, amino acid residues 277–289, 290–299, 294–333 and 300–316, suggesting these peptides are derived from trypsin-resistant fragments 276–414 and 294–414. Mass spectrometric analysis of the single broad band from FTLD-TDP type C identified the peptides of amino acids 273–283, 277–289, 290–313 and 317–330, strongly suggesting that the trypsin-resistant fragments from FTLD-TDP type C are derived from peptides 273–414 and 276–414. These analyses clearly indicate that trypsin-resistant core regions of the abnormal TDP-43 accumulated in the brain are not necessarily the same between ALS and FTLD (Supplementary Fig. 10).

Discussion

In this study, we have shown that the banding patterns for TDP-43 C-terminal fragments in ALS and FTLD are distinguishable and classifiable into at least three types. This difference was consistently demonstrated in 27 cases, eight with ALS, five with FTLD-TDP type A, eight with FTLD-TDP type B and six with FTLD-TDP type C. These results strongly suggest that distinct

types of TDP-43 molecules constitute the distinct types of pathologies of TDP-43 and determine the clinicopathological phenotypes of TDP-43 proteinopathies. In TDP-43 histopathology, ALS is considered to represent a distinct pathological subtype because the distribution of TDP-43 inclusions is different from that of FTLD-TDP (Mackenzie *et al.*, 2006a). However, as shown in this study, the TDP-43 accumulations in ALS and FTLD-TDP type B are biochemically indistinguishable. In fact, clinical and histopathological motor neuron disease is often present in cases with FTLD-TDP type B histology. In the three types of phosphorylated C-terminal TDP-43 banding pattern, the pattern seen in FTLD-TDP type C is the most distinctive, lacking the 26 kDa band detected in ALS, FTLD-TDP type A and type B cases (Fig. 1). The clinical diagnosis of the FTLD-TDP type C cases was semantic dementia in every instance, consistent with other studies showing this type of histology to be associated with semantic dementia (Mackenzie *et al.*, 2006a). FTLD is clinically classified into frontotemporal dementia, demantic dementia and progressive non-fluent aphasia, based on topographical distributions of degeneration (Neary *et al.*, 1998). In frontotemporal dementia, the bilateral frontal and temporal lobes are affected, whereas the bilateral temporal lobes are affected in semantic dementia and the left hemisphere in progressive non-fluent aphasia. Present data showing the most distinctive pattern of abnormal TDP-43 in type C indicate that semantic dementia may be biochemically different from frontotemporal dementia. Similar differences in tau fragment banding patterns have been shown between progressive supranuclear palsy and corticobasal degeneration (Arai *et al.*, 2004). Progressive supranuclear palsy and corticobasal degeneration are neurodegenerative diseases that are characterized by intracytoplasmic aggregates of hyperphosphorylated tau with four microtubule-binding repeats, with distinctive pathological features. Immunoblot analysis of Sarkosyl-insoluble tau demonstrated that a 33 kDa C-terminal fragment of tau band predominated in progressive supranuclear palsy, whereas two closely related bands of ~37 kDa predominated in corticobasal degeneration. The clinicopathological subtypes of these diseases may be explained by different conformations of protein aggregates or species of abnormal proteins.

Unfortunately, we were unable to obtain brain tissue samples from patients with FTLD-TDP type D (associated with *VCP* mutation; Cairns *et al.*, 2007b; Neumann *et al.*, 2007). However, because the deposition of abnormal TDP-43 in this disorder is mostly within neuronal nuclei, it is possible that the conformation of abnormal TDP-43 in FTLD-TDP type D may also differ from that in FTLD-TDP types A–C. Familial ALS and FTLD-TDP cases in which known mutations [*GRN* (Baker *et al.*, 2006) or *C9ORF72* (DeJesus-Hernandez *et al.*, 2011; Renton *et al.*, 2011)] were examined in this study. In FTLD-TDP due to *GRN* mutations, type A pathology is exclusively seen (Mackenzie *et al.*, 2006b; Cairns *et al.*, 2007b; Josephs *et al.*, 2007). All our cases with FTLD with *GRN* mutation showed the same C-terminal banding patterns of phosphorylated TDP-43 corresponding to type A histology. Some recent studies describing the clinical and pathological features of cases of FTLD-TDP with hexanucleotide repeat expansions in *C9ORF72* reported that many of the 'pure' frontotemporal dementia cases had type A pathology, whereas many of the combined frontotemporal dementia and motor neuron disease cases had type B pathology (Murray *et al.*, 2011; Boeve *et al.*, 2012; Hsiung *et al.*, 2012; Mahoney *et al.*, 2012; Simon-Sanchez *et al.*, 2012; Snowden *et al.*, 2012). Present cases with *C9ORF72* expansions included one case of ALS, one case of pure frontotemporal dementia with type A pathology, and two cases of frontotemporal dementia with motor neuron disease and type B pathology. The C-terminal banding pattern of these cases with familial ALS and frontotemporal dementia with motor neuron disease was not different from that in the sporadic ALS and FTLD-TDP type B cases, and that of the frontotemporal dementia case was not different from that in the cases with *GRN* mutation. Therefore, expansions in *C9ORF72* do not seem to influence the various types of TDP-43 C-terminal banding pattern or histological type of TDP-43 pathology.

Immunohistochemical studies using TDP-43 antibodies have shown that pathological TDP-43 is present throughout many CNS areas in ALS, suggesting that ALS does not selectively affect only the motor system, but is rather a multisystem neurodegenerative TDP-43 proteinopathy (Geser *et al.*, 2008). We also confirmed this viewpoint, immunohistochemically and biochemically, finding the same disease characteristic C-terminal fragment (banding) patterns of phosphorylated TDP-43 within the cerebral cortex, spinal cord and the other different brain regions in ALS. Although the types of pathological structures or their morphologies detected on immunohistochemistry analysis appeared different, the banding patterns for the C-terminal fragments were the same in all regions examined in three patients with ALS. This was also true for the one case with FTLD-TDP type C, where the same banding pattern of the C-terminal fragments was detected in several different brain regions beyond the frontal cortex (Fig. 3). These results strongly suggest that the same abnormal TDP-43 molecule is deposited in different brain regions in ALS (and probably also in FTLD-TDP type B) and FTLD-TDP type C, although we need to examine whether this is also true for cases with FTLD-TDP type A. Importantly, the extent of the abnormal protein pathology is closely correlated with the disease progression, such as Alzheimer's disease in tauopathies (Braak and Braak, 1991), and Parkinson's disease in α-synucleinopathies (Braak *et al.*, 2003; Saito *et al.*, 2003). However, the molecular mechanisms governing different clinicopathological phenotypes of these neurodegenerative diseases and their progression are poorly understood. Recent studies using cellular or animal models have suggested that aggregation-prone proteins, such as tau and α-synuclein, can spread to other cells and brain regions like prion disorders (Clavaguera *et al.*, 2009; Frost *et al.*, 2009; Nonaka *et al.*, 2010). The spreading of α-synuclein lesions to the grafts is also observed in Parkinson's disease brains after transplantation (Li *et al.*, 2008). However, it remains to be clarified whether the 'propagating' abnormal protein species represents a distinct 'strain type' that can be differentiated by molecular criteria in human patients or whether the species are the same in different brain regions.

We have also shown that the banding patterns of protease-resistant fragments of phosphorylated TDP-43 are similarly different in accordance with the banding patterns seen in untreated C-terminal fragments, confirming the direct link between neuropathological subtypes and biochemical banding patterns. The mass spectrometric analysis indicated that the protease resistant regions

of abnormal TDP-43 are different between the diseases. As abnormally phosphorylated TDP-43 has been shown to accumulate in a filamentous form in ALS spinal cords (Hasegawa *et al.*, 2008), the filament core regions may be different between the diseases. Protease-resistant bands, and differences in banding patterns, have been reported in the prion diseases, Creutzfeldt–Jakob disease and bovine spongiform encephalopathy (Collinge *et al.*, 1996). Protease-resistant prion protein extracted from cases with new-variant Creutzfeldt–Jakob disease showed a different and characteristic pattern from that in cases with sporadic Creutzfeldt–Jakob disease, with the banding pattern being indistinguishable from that of mice infected with bovine spongiform encephalopathy prion. Protease-treated prion protein species are thought to have different mobilities because of different conformations. These observations in prion disease suggest that the different banding patterns to the abnormal TDP-43 fragments in ALS and FTLD might represent different TDP-43 strains with different conformations.

Recently, TDP-43 pathology has been detected in some cases with Alzheimer's disease (Arai *et al.*, 2009). We have shown here that the banding patterns of TDP-43 in cases of Alzheimer's disease with TDP-43 pathology are the same as those in FTLD-TDP type A. These novel observations suggest a biochemical commonality between FTLD and Alzheimer's disease with respect to TDP-43 pathology.

The results shown in this study also suggest a molecular basis for the clinicopathological classification of TDP-43 proteinopathies, which complements the histological classifications (Mackenzie *et al.*, 2011).

Funding

This work was supported by a Grant-in-Aid for Scientific Research (A) (to M.H., 11000624) from Ministry of Education, Culture, Sports, Science and Technology of Japan, and grants from Ministry of Health, Labor and Welfare of Japan (to M.H.).

Supplementary material

Supplementary material is available at *Brain* online.

References

Arai T, Mackenzie IR, Hasegawa M, Nonoka T, Niizato K, Tsuchiya K, et al. Phosphorylated TDP-43 in Alzheimer's disease and dementia with Lewy bodies. Acta Neuropathol (Berl) 2009; 117: 125–36.

Arai T, Hasegawa M, Akiyama H, Ikeda K, Nonaka T, Mori H, et al. TDP-43 is a component of ubiquitin-positive tau-negative inclusions in frontotemporal lobar degeneration and amyotrophic lateral sclerosis. Biochem Biophys Res Commun 2006; 351: 602–11.

Arai T, Ikeda K, Akiyama H, Nonaka T, Hasegawa M, Ishiguro K, et al. Identification of amino-terminally cleaved tau fragments that distinguish progressive supranuclear palsy from corticobasal degeneration. Ann Neurol 2004; 55: 72–9.

Armstrong RA, Ellis W, Hamilton RL, Mackenzie IR, Hedreen J, Gearing M, et al. Neuropathological heterogeneity in frontotemporal lobar degeneration with TDP-43 proteinopathy: a quantitative study of 94 cases using principal components analysis. J Neural Transm 2010; 117: 227–39.

Baker M, Mackenzie IR, Pickering-Brown SM, Gass J, Rademakers R, Lindholm C, et al. Mutations in progranulin cause tau-negative frontotemporal dementia linked to chromosome 17. Nature 2006; 442: 916–19.

Boeve BF, Boylan KB, Graff-Radford NR, Dejesus-Hernandez M, Knopman DS, Pedraza O, et al. Characterization of frontotemporal dementia and/or amyotrophic lateral sclerosis associated with the GGGGCC repeat expansion in *C9ORF72*. Brain 2012; 135: 765–83.

Braak H, Braak E. Neuropathological stageing of Alzheimer-related changes. Acta Neuropathol 1991; 82: 239–59.

Braak H, Del Tredici K, Rub U, de Vos RA, Jansen Steur EN, Braak E. Staging of brain pathology related to sporadic Parkinson's disease. Neurobiol Aging 2003; 24: 197–211.

Brooks BR. El Escorial World Federation of Neurology criteria for the diagnosis of amyotrophic lateral sclerosis. Subcommittee on Motor Neuron Diseases/Amyotrophic Lateral Sclerosis of the World Federation of Neurology Research Group on Neuromuscular Diseases and the El Escorial "Clinical limits of amyotrophic lateral sclerosis" workshop contributors. J Neurol Sci 1994; 124 (Suppl): 96–107.

Cairns NJ, Bigio EH, Mackenzie IR, Neumann M, Lee VM, Hatanpaa KJ, et al. Neuropathologic diagnostic and nosologic criteria for frontotemporal lobar degeneration: consensus of the Consortium for Frontotemporal Lobar Degeneration. Acta Neuropathol 2007a; 114: 5–22.

Cairns NJ, Neumann M, Bigio EH, Holm IE, Troost D, Hatanpaa KJ, et al. TDP-43 in familial and sporadic frontotemporal lobar degeneration with ubiquitin inclusions. Am J Pathol 2007b; 171: 227–40.

Clavaguera F, Bolmont T, Crowther RA, Abramowski D, Frank S, Probst A, et al. Transmission and spreading of tauopathy in transgenic mouse brain. Nat Cell Biol 2009; 11: 909–13.

Collinge J, Sidle KC, Meads J, Ironside J, Hill AF. Molecular analysis of prion strain variation and the aetiology of 'new variant' CJD. Nature 1996; 383: 685–90.

DeJesus-Hernandez M, Mackenzie IR, Boeve BF, Boxer AL, Baker M, Rutherford NJ, et al. Expanded GGGGCC hexanucleotide repeat in noncoding region of *C9ORF72* causes chromosome 9p-linked FTD and ALS. Neuron 2011; 72: 245–56.

Frost B, Jacks RL, Diamond MI. Propagation of tau misfolding from the outside to the inside of a cell. J Biol Chem 2009; 284: 12845–52.

Geser F, Brandmeir NJ, Kwong LK, Martinez-Lage M, Elman L, McCluskey L, et al. Evidence of multisystem disorder in whole-brain map of pathological TDP-43 in amyotrophic lateral sclerosis. Arch Neurol 2008; 65: 636–41.

Geser F, Martinez-Lage M, Robinson J, Uryu K, Neumann M, Brandmeir NJ, et al. Clinical and pathological continuum of multisystem TDP-43 proteinopathies. Arch Neurol 2009; 66: 180–9.

Gitcho MA, Bigio EH, Mishra M, Johnson N, Weintraub S, Mesulam M, et al. TARDBP 3'-UTR variant in autopsy-confirmed frontotemporal lobar degeneration with TDP-43 proteinopathy. Acta Neuropathol 2009; 118: 633–45.

Hasegawa M, Arai T, Nonaka T, Kametani F, Yoshida M, Hashizume Y, et al. Phosphorylated TDP-43 in frontotemporal lobar degeneration and amyotrophic lateral sclerosis. Ann Neurol 2008; 64: 60–70.

Hsiung GY, Dejesus-Hernandez M, Feldman HH, Sengdy P, Bouchard-Kerr P, Dwosh E, et al. Clinical and pathological features of familial frontotemporal dementia caused by *C9ORF72* mutation on chromosome 9p. Brain 2012; 135: 709–22.

Inukai Y, Nonaka T, Arai T, Yoshida M, Hashizume Y, Beach TG, et al. Abnormal phosphorylation of Ser409/410 of TDP-43 in FTLD-U and ALS. FEBS Lett 2008; 582: 2899–904.

Josephs KA, Ahmed Z, Katsuse O, Parisi JF, Boeve BF, Knopman DS, et al. Neuropathologic features of frontotemporal lobar degeneration with ubiquitin-positive inclusions with progranulin gene (*GRN*) mutations. J Neuropathol Exp Neurol 2007; 66: 142–51.

Kabashi E, Valdmanis PN, Dion P, Spiegelman D, McConkey BJ, Vande Velde C, et al. TARDBP mutations in individuals with sporadic and familial amyotrophic lateral sclerosis. Nat Genet 2008; 40: 572–4.

Kovacs GG, Murrell JR, Horvath S, Haraszti L, Majtenyi K, Molnar MJ, et al. TARDBP variation associated with frontotemporal dementia, supranuclear gaze palsy, and chorea. Mov Disord 2009; 24: 1843–7.

Li JY, Englund E, Holton JL, Soulet D, Hagell P, Lees AJ, et al. Lewy bodies in grafted neurons in subjects with Parkinson's disease suggest host-to-graft disease propagation. Nat Med 2008; 14: 501–3.

Mackenzie IR, Baborie A, Pickering-Brown S, Du Plessis D, Jaros E, Perry RH, et al. Heterogeneity of ubiquitin pathology in frontotemporal lobar degeneration: classification and relation to clinical phenotype. Acta Neuropathol 2006a; 112: 539–49.

Mackenzie IR, Baker M, Pickering-Brown S, Hsiung GY, Lindholm C, Dwosh E, et al. The neuropathology of frontotemporal lobar degeneration caused by mutations in the progranulin gene. Brain 2006b; 129: 3081–90.

Mackenzie IR, Neumann M, Baborie A, Sampathu DM, Du Plessis D, Jaros E, et al. A harmonized classification system for FTLD-TDP pathology. Acta Neuropathol 2011; 122: 111–13.

Mahoney CJ, Beck J, Rohrer JD, Lashley T, Mok K, Shakespeare T, et al. Frontotemporal dementia with the *C9ORF72* hexanucleotide repeat expansion: clinical, neuroanatomical and neuropathological features. Brain 2012; 135: 736–50.

Murray ME, DeJesus-Hernandez M, Rutherford NJ, Baker M, Duara R, Graff-Radford NR, et al. Clinical and neuropathologic heterogeneity of c9FTD/ALS associated with hexanucleotide repeat expansion in *C9ORF72*. Acta Neuropathol 2011; 122: 673–90.

Neary D, Snowden JS, Gustafson L, Passant U, Stuss D, Black S, et al. Frontotemporal lobar degeneration: a consensus on clinical diagnostic criteria. Neurology 1998; 51: 1546–54.

Neumann M, Mackenzie IR, Cairns NJ, Boyer PJ, Markesbery WR, Smith CD, et al. TDP-43 in the ubiquitin pathology of frontotemporal dementia with *VCP* gene mutations. J Neuropathol Exp Neurol 2007; 66: 152–7.

Neumann M, Sampathu DM, Kwong LK, Truax AC, Micsenyi MC, Chou TT, et al. Ubiquitinated TDP-43 in frontotemporal lobar degeneration and amyotrophic lateral sclerosis. Science 2006; 314: 130–3.

Nonaka T, Watanabe ST, Iwatsubo T, Hasegawa M. Seeded aggregation and toxicity of α-synuclein and tau: cellular models of neurodegenerative diseases. J Biol Chem 2010; 285: 34885–98.

Renton AE, Majounie E, Waite A, Simon-Sanchez J, Rollinson S, Gibbs JR, et al. A hexanucleotide repeat expansion in *C9ORF72* is the cause of chromosome 9p21-linked ALS-FTD. Neuron 2011; 72: 257–68.

Saito Y, Kawashima A, Ruberu NN, Fujiwara H, Koyama S, Sawabe M, et al. Accumulation of phosphorylated alpha-synuclein in aging human brain. J Neuropathol Exp Neurol 2003; 62: 644–54.

Simon-Sanchez J, Dopper EG, Cohn-Hokke PE, Hukema RK, Nicolaou N, Seelaar H, et al. The clinical and pathological phenotype of *C9ORF72* hexanucleotide repeat expansions. Brain 2012; 135: 723–35.

Snowden JS, Rollinson S, Thompson JC, Harris JM, Stopford CL, Richardson AM, et al. Distinct clinical and pathological characteristics of frontotemporal dementia associated with *C9ORF72* mutations. Brain 2012; 135: 693–708.

Sreedharan J, Blair IP, Tripathi VB, Hu X, Vance C, Rogelj B, et al. TDP-43 mutations in familial and sporadic amyotrophic lateral sclerosis. Science 2008; 319: 1668–72.

Tan CF, Eguchi H, Tagawa A, Onodera O, Iwasaki T, Tsujino A, et al. TDP-43 immunoreactivity in neuronal inclusions in familial amyotrophic lateral sclerosis with or without SOD1 gene mutation. Acta Neuropathol 2007; 113: 535–42.

STEM CELLS

Drug Screening for ALS Using Patient-Specific Induced Pluripotent Stem Cells

Naohiro Egawa,[1,2]* Shiho Kitaoka,[1,2]* Kayoko Tsukita,[1,2] Motoko Naitoh,[3] Kazutoshi Takahashi,[1] Takuya Yamamoto,[1,4] Fumihiko Adachi,[1] Takayuki Kondo,[1,5] Keisuke Okita,[1] Isao Asaka,[1] Takashi Aoi,[1] Akira Watanabe,[1,4] Yasuhiro Yamada,[1,4] Asuka Morizane,[1,6] Jun Takahashi,[1,6] Takashi Ayaki,[5] Hidefumi Ito,[5] Katsuhiro Yoshikawa,[3] Satoko Yamawaki,[3] Shigehiko Suzuki,[3] Dai Watanabe,[7] Hiroyuki Hioki,[8] Takeshi Kaneko,[8] Kouki Makioka,[9] Koichi Okamoto,[9] Hiroshi Takuma,[10] Akira Tamaoka,[10] Kazuko Hasegawa,[11] Takashi Nonaka,[12] Masato Hasegawa,[12] Akihiro Kawata,[13] Minoru Yoshida,[14] Tatsutoshi Nakahata,[1] Ryosuke Takahashi,[5] Maria C. N. Marchetto,[15] Fred H. Gage,[15] Shinya Yamanaka,[1,4,16] Haruhisa Inoue[1,2,16]†

Amyotrophic lateral sclerosis (ALS) is a late-onset, fatal disorder in which the motor neurons degenerate. The discovery of new drugs for treating ALS has been hampered by a lack of access to motor neurons from ALS patients and appropriate disease models. We generate motor neurons from induced pluripotent stem cells (iPSCs) from familial ALS patients, who carry mutations in Tar DNA binding protein-43 (TDP-43). ALS patient–specific iPSC–derived motor neurons formed cytosolic aggregates similar to those seen in postmortem tissue from ALS patients and exhibited shorter neurites as seen in a zebrafish model of ALS. The ALS motor neurons were characterized by increased mutant TDP-43 protein in a detergent-insoluble form bound to a spliceosomal factor SNRPB2. Expression array analyses detected small increases in the expression of genes involved in RNA metabolism and decreases in the expression of genes encoding cytoskeletal proteins. We examined four chemical compounds and found that a histone acetyltransferase inhibitor called anacardic acid rescued the abnormal ALS motor neuron phenotype. These findings suggest that motor neurons generated from ALS patient–derived iPSCs may provide a useful tool for elucidating ALS disease pathogenesis and for screening drug candidates.

INTRODUCTION

Amyotrophic lateral sclerosis (ALS) is a neurodegenerative disorder characterized by a loss of upper and lower motor neurons that typically develops in the fifth or sixth decade of life, with a survival of less than 5 years and a prevalence of 2 in 100,000 (*1*, *2*). The histopathological hallmarks of this fatal disease include cytosolic aggregates in the motor neurons of most ALS patients with the sporadic form of the disease. These aggregates are composed of Tar DNA binding protein-43 (TDP-43) (*3*–*5*), a 414–amino acid nuclear mRNA binding protein containing two RNA recognition motifs. Genetic analysis has identified more than 30 mutations in the *TDP-43* gene in both familial and sporadic ALS cases (*6*). ALS-associated abnormalities have been reported in patient samples and cellular and animal models (*6*–*10*), and several compounds have been identified as abrogating the disease phenotype in an ALS mouse model. However, when these compounds were tested in ALS patients, no clinical improvements were observed (*11*).

Induced pluripotent stem cells (iPSCs) have been generated from ALS patients and differentiated into motor neurons (*12*, *13*), but it is not yet clear whether the abnormal cellular and molecular phenotypes of ALS can be recapitulated in vitro. A lack of access to human motor neurons and appropriate disease models has hampered efforts to test new drug candidates for ALS. Here, we generated human motor neurons from iPSCs derived from familial ALS patients carrying *TDP-43* mutations and used them to identify a compound that rescued the ALS-associated phenotype.

RESULTS

Spinal motor neurons were generated from iPSCs derived from dermal fibroblasts from patients with familial ALS or from control individuals by means of retroviral or episomal vectors. Seven control human iPSC lines were derived from five unrelated individuals without mutations in the *TDP-43* gene, and nine ALS iPSC lines were generated from three ALS patients with mutations in *TDP-43* (*14*, *15*) (Fig. 1A, fig. S1A, and table S1). ALS patients A21, A34, and ND32947 were heterozygous for the Q343R, M337V, and G298S mutations in *TDP-43*, respectively. Neural populations including motor neurons derived from the ALS patient iPSCs retained these *TDP-43* mutations (Fig. 1B).

[1]Center for iPS Cell Research and Application (CiRA), Kyoto University, Kyoto 606-8507, Japan. [2]Core Research for Evolutional Science and Technology (CREST), Japan Science and Technology Agency, Tokyo 102-0076, Japan. [3]Department of Plastic and Reconstructive Surgery, Graduate School of Medicine, Kyoto University, Kyoto 606-8507, Japan. [4]Institute for Integrated Cell-Material Sciences, Kyoto University, Kyoto 606-8501, Japan. [5]Department of Neurology, Graduate School of Medicine, Kyoto University, Kyoto 606-8507, Japan. [6]Department of Biological Repair, Institute for Frontier Medical Sciences, Kyoto University, Kyoto 606-8507, Japan. [7]Department of Biological Sciences, Graduate School of Medicine and Department of Molecular and Systems Biology, Graduate School of Biostudies, Kyoto University, Kyoto 606-8501, Japan. [8]Department of Morphological Brain Science, Graduate School of Medicine, Kyoto University, Kyoto 606-8501, Japan. [9]Department of Neurology, Gunma University Graduate School of Medicine, Maebashi 371-8511, Japan. [10]Department of Neurology, Institute of Clinical Medicine, University of Tsukuba, Tsukuba 305-8576, Japan. [11]Department of Neurology, Sagamihara Hospital, Sagamihara 252-0392, Japan. [12]Department of Neuropathology and Cell Biology, Tokyo Metropolitan Institute of Medical Science, Tokyo 156-8506, Japan. [13]Department of Neurology, Tokyo Metropolitan Neurological Hospital, Tokyo 183-0042, Japan. [14]Chemical Genetics Laboratory Molecular Ligand Biology Research Team, Chemical Genomics Research Group, RIKEN Advanced Science Institute, Wako, Saitama 351-0198, Japan. [15]The Salk Institute for Biological Studies, La Jolla, CA 92037, USA. [16]Yamanaka iPS Cell Special Project, Japan Science and Technology Agency, Kawaguchi 332-0012, Japan.
*These authors contributed equally to this work.
†To whom correspondence should be addressed. E-mail: haruhisa@cira.kyoto-u.ac.jp

The iPSCs generated from ALS and control dermal fibroblasts expressed human embryonic stem cell (ESC) markers (Fig. 1A and fig. S1A) and were fully characterized (figs. S1 to S5 and table S2). The ALS and control iPSC lines were then differentiated into motor neurons (*16*) (Fig. 1C and fig. S6A). Differentiated motor neurons were identified by expression of motor neuron markers including Islet-1, HB9, SMI-32, and ChAT (choline acetyltransferase) (Fig. 1C and fig. S6B), and their function was verified by coculture with myotubes (fig. S6, D to F). To visualize live motor neurons, we transduced them with lentivirus expressing green fluorescent protein (GFP) under the control of the HB9 promoter (HB9::GFP) (*17*) (Fig. 1C). HB9::GFP-positive neurons colocalized with ChAT (fig. S6C) and showed spontaneous action potentials and synaptic potentials (fig. S6, G to K). Immunocytochemical analysis with MAP2, SMI-32, and GFAP (glial fibrillary acidic protein) did not reveal any differences in differentiation propensity between ALS and control iPSCs (Fig. 1, D to G, and fig. S7).

Next, we examined whether ALS iPSC–derived motor neurons have shorter neurites as reported in an ALS zebrafish model (*6*) and decreased neurofilament mRNA as reported in postmortem tissues from ALS patients (*7*, *18*). ALS iPSC–derived motor neurons expressing HB9::GFP were purified by fluorescence-activated cell sorting (FACS) (*17*, *19*) (Fig. 2A and fig. S8, A to C). ALS iPSC–derived motor neurons showed shorter neurites [33.5 ± 9.9 μm (mean ± SD) compared to 63.8 ± 13.1 μm for control; $P = 2.0 \times 10^{-4}$ by *t* test] (Fig. 2, A and B, and fig. S9A). Gene expression profiling of the purified ALS iPSC–derived motor neurons showed that there was a decrease in expression of genes encoding components of cytoskeletal intermediate filaments (control > ALS, fold change >1.2, $P < 0.01$) (Fig. 2D, fig. S8, F and G, and table S4). The expression of medium polypeptide neurofilament (NEFM) and light polypeptide neurofilament (NEFL) was significantly decreased in ALS compared to control iPSC–derived motor neurons [$P = 7.9 \times 10^{-3}$ (NEFL); $P = 5.3 \times 10^{-3}$ (NEFM); *t* test] (Fig. 2C and table S6).

TDP-43 is involved in multiple steps of RNA metabolism, including transcription, splicing, and transport of mRNA (*20*–*22*). TDP-43 protein autoregulates its synthesis by binding to the 3′ untranslated region of its own mRNA in a negative feedback loop (*8*). Gene expression profiles of purified ALS iPSC–derived motor neurons demonstrated that gene ontology (GO) terms related to RNA binding, splicing, processing, and transcriptional initiation were enriched compared to the profiles of control iPSC–derived motor neurons (Fig. 2D). The transcripts of nuclear transport/RNA granule and spliceosomal complex–related genes were also up-regulated in ALS iPSC–derived motor neurons (Fig. 2D, fig. S8, D, E, and G, and tables S3 and S5), indicating that RNA metabolism may be perturbed in ALS compared to control iPSC–derived motor

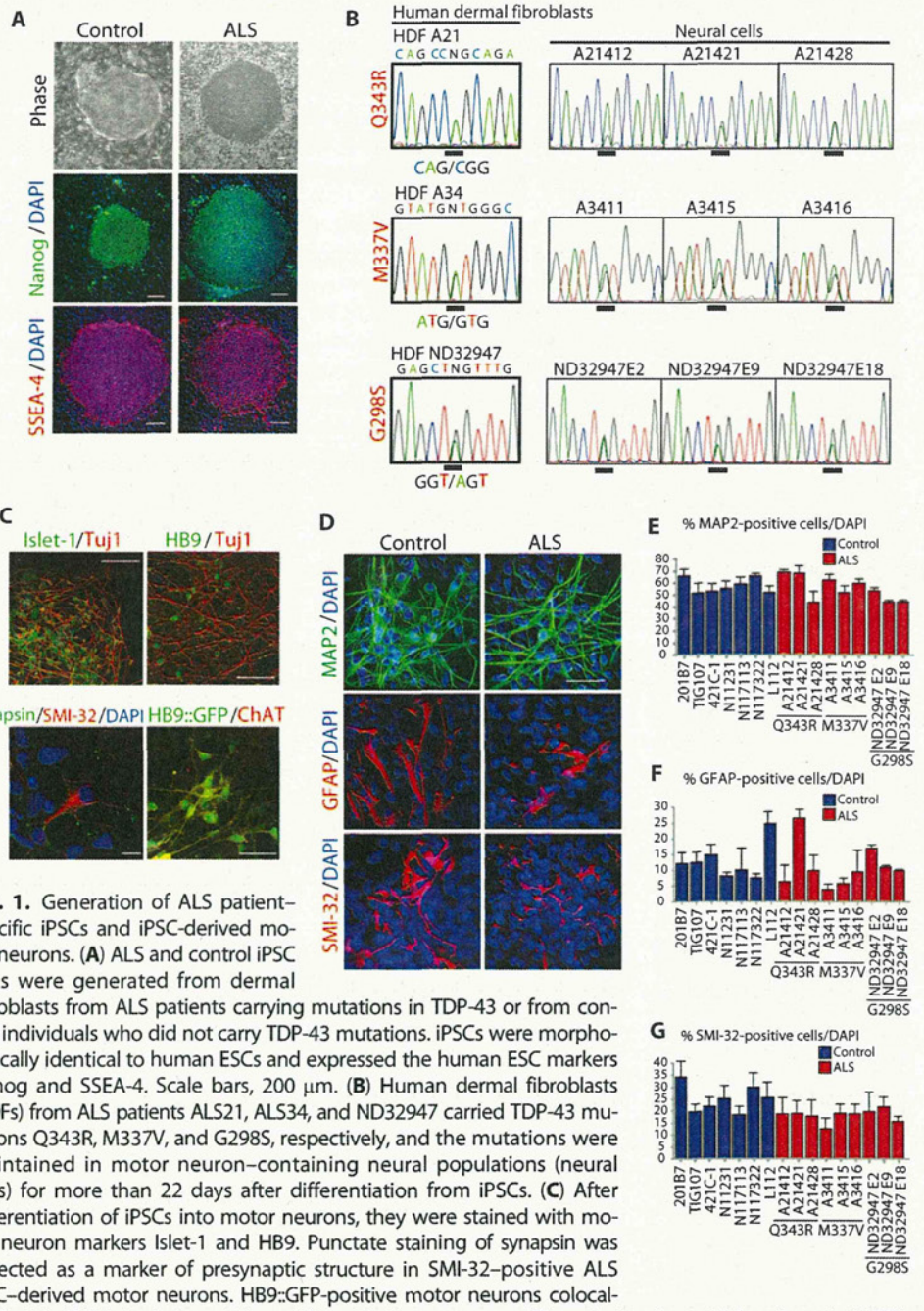

Fig. 1. Generation of ALS patient–specific iPSCs and iPSC-derived motor neurons. (**A**) ALS and control iPSC lines were generated from dermal fibroblasts from ALS patients carrying mutations in TDP-43 or from control individuals who did not carry TDP-43 mutations. iPSCs were morphologically identical to human ESCs and expressed the human ESC markers Nanog and SSEA-4. Scale bars, 200 μm. (**B**) Human dermal fibroblasts (HDFs) from ALS patients ALS21, ALS34, and ND32947 carried TDP-43 mutations Q343R, M337V, and G298S, respectively, and the mutations were maintained in motor neuron–containing neural populations (neural cells) for more than 22 days after differentiation from iPSCs. (**C**) After differentiation of iPSCs into motor neurons, they were stained with motor neuron markers Islet-1 and HB9. Punctate staining of synapsin was detected as a marker of presynaptic structure in SMI-32–positive ALS iPSC–derived motor neurons. HB9::GFP-positive motor neurons colocalized with ChAT. Scale bars, 50 μm. (**D** to **G**) Motor neuron differentiation from ALS and control iPSCs. After 2 months of differentiation from iPSCs in culture, motor neurons were stained with the MAP2 neuronal marker and the motor neuron–specific marker SMI-32. Astrocytes were revealed by staining with GFAP. Scale bar, 50 μm. Proportions of ALS and control iPSC–derived motor neurons staining positive for MAP2 (E), GFAP (F), and SMI-32 (G) are shown. Error bars are SD.

neurons (*8*, *20*). The expression of TDP-43 mRNA was significantly increased in ALS iPSC–derived motor neurons compared to control ($P = 0.040$ by t test; Fig. 2E and fig. S8, D and G) (*8*, *23*).

TDP-43 has been reported in the detergent-insoluble fraction of postmortem tissues from ALS patients (*3*, *4*, *24*) and has been shown to be mislocalized, forming cytoplasmic preinclusions (*20*). To analyze the biochemical properties of TDP-43 in ALS iPSC–derived neural populations containing motor neurons, we performed Western blot analysis. The amount of detergent-insoluble TDP-43 including full-length and smaller fragments increased markedly in ALS iPSC–derived motor neuron–containing neural populations (Fig. 2F and fig. S9B). Immunocytochemical analysis revealed that TDP-43 in control

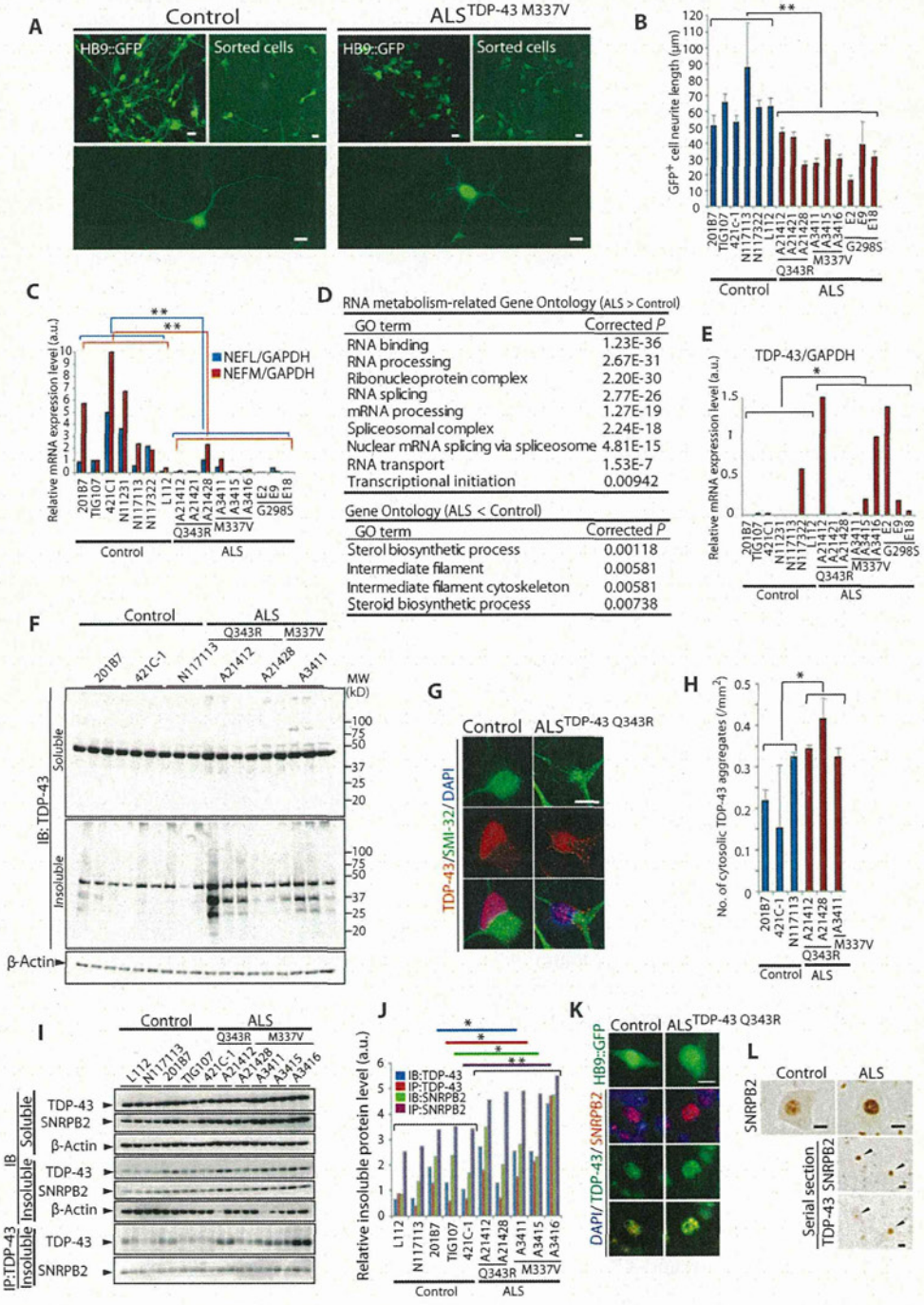

Fig. 2. Phenotypes of ALS iPSC–derived motor neurons. (**A**) ALS iPSC–derived HB9::GFP-positive motor neurons are shown before and after sorting by FACS. (Lower panels) Representative images of purified ALS and control iPSC–derived motor neurons. Scale bars, 10 μm. (**B**) The length of neurites was measured in purified ALS and control iPSC–derived motor neurons. $P = 2.0 \times 10^{-4}$ by t test. Error bars are SEM. (**C**) The expression of NEFL and NEFM was decreased in ALS versus control iPSC–derived motor neurons. $P = 7.9 \times 10^{-3}$, NEFL; $P = 5.3 \times 10^{-3}$, NEFM by t test. (**D**) Major GO terms showed both increases and decreases in gene expression in ALS versus control iPSC–derived motor neurons. (**E**) qPCR showed increased expression of TDP-43 mRNA relative to glyceraldehyde-3-phosphate dehydrogenase (GAPDH) mRNA in ALS versus control iPSC–derived motor neurons. $P = 0.040$ by t test. (**F**) Soluble (upper panel) and insoluble (lower panel) TDP-43 fractions from ALS and control iPSC–derived motor neuron–containing neural populations. (**G**) ALS and control iPSC–derived motor neurons were immunostained for TDP-43 and for the SMI-32 motor neuron marker; DAPI nuclear stain, blue. Scale bars, 10 μm. (**H**) Number of TDP-43–positive cytosolic aggregates measured by high-content analysis. $P = 0.0458$ by t test. Error bars are SEM. (**I**) Immunoblots of different proteins including TDP-43 with antibodies against indicated proteins. Insoluble TDP-43 was immunoprecipitated (IP) from the insoluble fraction and immunoblotted (IB) with each antibody. (**J**) Quantification of protein band densities of TDP-43 and SNRPB2 in insoluble fractions from total lysates and in TDP-43–immunoprecipitated insoluble fractions relative to β-actin. $P = 0.034$ (TDP-43 in the insoluble fraction from total lysates of ALS compared to control motor neuron–containing neural populations) by t test; $P = 1.0 \times 10^{-4}$ (SNRPB2 coimmunoprecipitated with TDP-43 in ALS compared to control motor neuron–containing neural populations) by t test. (**K**) HB9::GFP-labeled ALS and control iPSC–derived motor neurons were immunostained for SNRPB2 and TDP-43 and counterstained with DAPI nuclear stain (blue). Scale bar, 10 μm. (**L**) Representative images showing immunostaining for SNRPB2 in postmortem spinal cord tissue from ALS patients or control individuals. Arrowheads, ALS spinal cord tissue immunoreactive for both TDP-43 and SNRPB2 in serial sections. Scale bars, 10 μm. *$P < 0.05$, **$P < 0.01$.

iPSC–derived motor neurons was mainly localized in the nucleus, whereas TDP-43 in ALS iPSC–derived motor neurons was distributed in both the nucleus and the cytoplasm (Fig. 2G), with TDP-43 in the cytoplasm forming preinclusion-like aggregates. High-content analysis revealed that the number of such TDP-43 aggregates in ALS motor neurons was increased compared to that in control motor neurons ($P = 0.0458$ by t test; Fig. 2H).

Next, we analyzed SNRPB2, a highly expressed spliceosomal factor, in ALS iPSC–derived motor neurons (fig. S8E). The amount of TDP-43 protein was increased ($P = 0.034$ by t test; Fig. 2, I and J), and the amount of SNRPB2 bound to TDP-43 was increased ($P = 1.0 \times 10^{-4}$ by t test; Fig. 2, I and J) in the insoluble fraction of ALS iPSC–derived motor neuron–containing neural populations compared to control. TDP-43 colocalized with SNRPB2 to form aggregates in the nucleus of ALS iPSC–derived motor neurons (Fig. 2K) and motor neurons from postmortem tissue from ALS patients (Fig. 2L).

Next, we established an assay to measure death of ALS iPSC–derived motor neurons in response to arsenite, which induces oxidative stress and an increase in the amount of insoluble TDP-43 in these motor neurons (*25*). Arsenite increased the amount of TDP-43 in the insoluble fraction of ALS iPSC–derived motor neuron–containing neural populations [$P = 7.8 \times 10^{-3}$ by two-way analysis of variance (ANOVA); Fig. 3, A and B]. The number of surviving ALS iPSC–derived motor neurons was lower compared to control iPSC–derived motor neurons (18% reduction in ALS motor neurons relative to control; $P = 5.0 \times 10^{-4}$ by two-way ANOVA) (Fig. 3, C and D). Staining with ethidium homodimer-1, which selectively permeates the broken membranes of dying cells, revealed that the proportion of dying ALS iPSC–derived motor neurons was greater than that of control iPSC–derived motor neurons [33.5 ± 1.9% (mean ± SD) for ALS compared to 16.1 ± 3.0% for control; $P = 2.9 \times 10^{-3}$ by two-way ANOVA] (Fig. 3, E and F).

Given that gene expression analysis suggested that transcription and RNA splicing were perturbed in ALS iPSC–derived motor neurons, we tested four drugs that had been reported to modulate transcription through histone modification or RNA

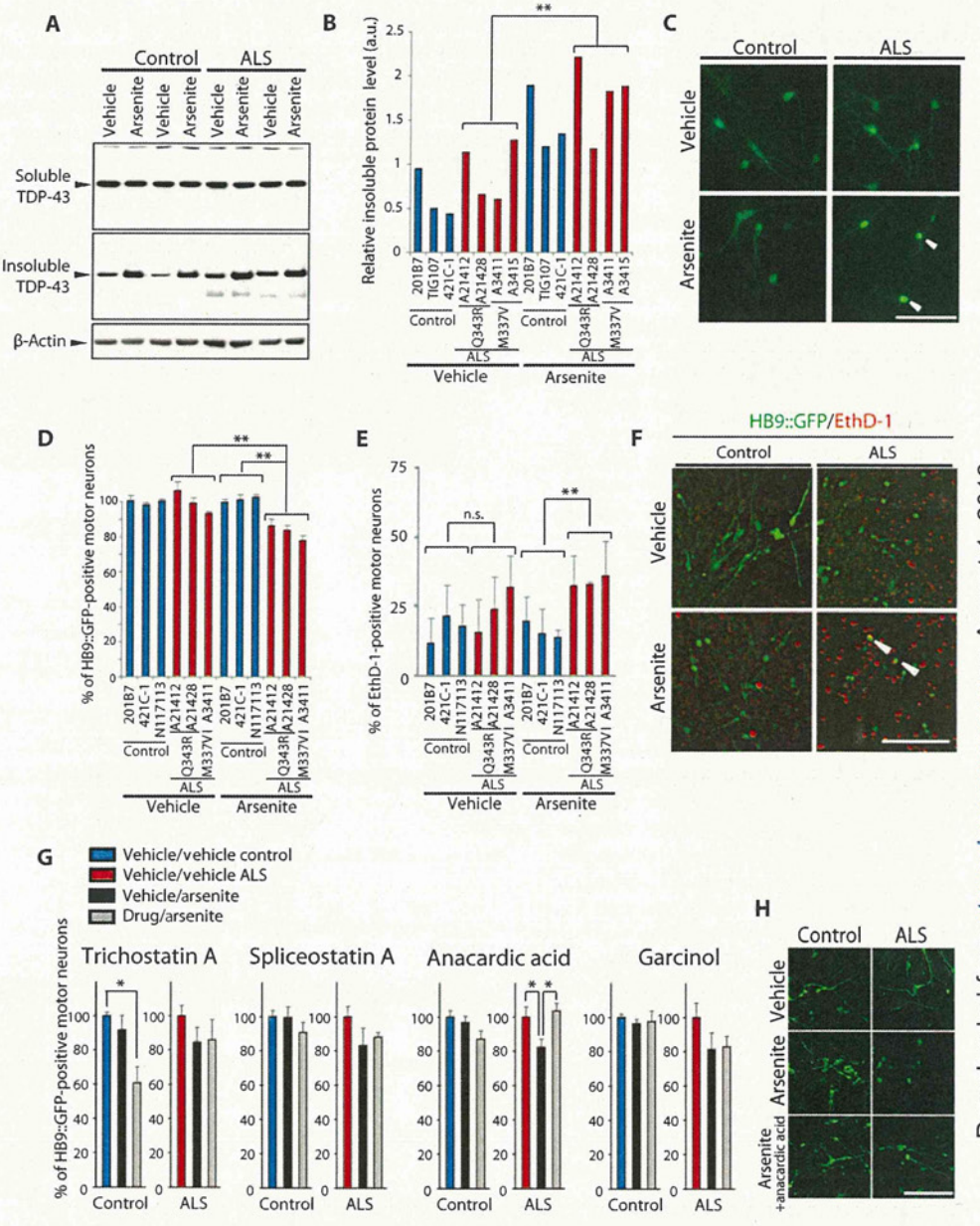

Fig. 3. Arsenite-induced death of ALS and control iPSC–derived motor neurons. (**A** and **B**) Decreased solubility of TDP-43 after treatment with arsenite. (A) After treatment with vehicle or arsenite (0.5 mM, 1 hour), cell lysates were separated into soluble and insoluble fractions and immunoblotted with TDP-43 antibody. (B) Arsenite increased the amount of TDP-43 in the insoluble fraction in ALS iPSC–derived motor neurons ($n = 4$) compared to control ($n = 3$). $P = 7.8 \times 10^{-3}$ by two-way ANOVA. (**C**) Images of control versus ALS iPSC–derived motor neurons after treatment with vehicle or arsenite. Arrowheads, dying motor neurons. Scale bar, 100 μm. (**D**) Proportion of HB9::GFP-positive control and ALS iPSC–derived motor neurons after treatment with vehicle or arsenite. $P = 5.0 \times 10^{-4}$ by two-way ANOVA. Error bars are SEM. (**E**) Death of motor neurons was assessed by ethidium homodimer-1 (EthD-1) uptake after incubation with vehicle or arsenite. $P = 2.9 \times 10^{-3}$ by two-way ANOVA. Error bars are SEM. (**F**) Images of ALS versus control iPSC–derived motor neurons after arsenite treatment. Scale bar, 100 μm. (**G**) Treatment with 5 μM anacardic acid ($n = 6$) for 16 hours blocked arsenite-induced death of ALS iPSC–derived motor neurons. Trichostatin A (3 μM) ($n = 3$), spliceostatin A (100 ng/ml) ($n = 3$), and garcinol (5 μM) ($n = 6$) failed to block arsenite-induced cell death. $P = 0.048$ by one-way ANOVA. Error bars are SEM. (**H**) Images of anacardic acid–treated motor neurons followed by arsenite treatment. Scale bar, 100 μm. *$P < 0.05$, **$P < 0.01$.